Available online at www.sciencedirect.com
SCIENCE DIRECT®
Journal of Power Sources 147 (2005) 116–127
JOURNAL OF POWER SOURCES
www.elsevier.com/locate/jpowsour

A radial microfluidic fuel processor

Ashish V. Pattekar, Mayuresh V. Kothare*

Integrated Microchemical Systems Laboratory, Department of Chemical Engineering, Lehigh University, 111 Research Drive, Bethlehem, PA 18015, USA

Received 13 December 2004; accepted 14 January 2005
Available online 14 April 2005

Abstract

A novel radial flow packed-bed microreactor has been developed to enable hydrogen delivery in miniature fuel cells for portable power generation using the methanol reforming process. Conventional rectangular microchannel based designs typically used for on-chip chemical processing were found to be inadequate for practical high-throughput micro packed-bed application due to the associated high pressure drops. The radial design exploits several physical phenomena inherent to the device operation and provides an order of magnitude reduction in the required driving pressure while maintaining the compact design of the microreactor and providing greater than 98% conversion of methanol to hydrogen at flow rates sufficient to supply hydrogen to a 20 W fuel cell. The developed microreactor opens the path for fuel cell based portable energy systems with energy storage capacities up to 10 times those possible with current battery technology.

Keywords: Microreactor; Micro fuel cells; Microreformer; Microfluidics; Lab-on-a-chip; Radial flow

1. Introduction and literature survey

Miniaturized 'lab-on-a-chip' and 'plant-on-a-chip' devices have been successfully developed for several real-world applications in recent years [1–4]. *Power-plant-on-chip* and *palm power* are buzzwords of great interest currently in the micro-power community where battery technology is thought to be quickly approaching its peak in energy storage capacity per unit volume/weight of the power source [5]. As a promising alternative, hydrogen fuel cells have long been considered a power source of the future due to their high efficiency in the conversion of fuel to usable energy and low emission of pollutants and greenhouse gases during operation [6,7]. In the context of portable and *palm* power sources, fuel cells have the potential of providing energy storage densities several times those possible using current state-of-the-art lithium-ion batteries [5]. However, the difficulties and hazards involved in the storage and handling of the hydrogen fuel in either compressed gas or liquid form have been a major impediment in the successful commercialization of miniature hydrogen proton exchange membrane (PEM) fuel cells. Also, the stored energy density of hydrogen in compressed or liquid form is significantly lower in comparison to storage in the form of liquid hydrocarbons, such as methanol, which can be reformed for generation of the hydrogen gas as and when needed. Hydrogen storage in metal hydrides and nanostructured carbon [8,9] has been proposed but a number of limitations have been recognized, including high weight of the hydride storage unit, lower energy density, the passive nature of the hydrogen release mechanism and high cost. Therefore, the development of a compact and efficient miniaturized fuel 'reformer' for on-demand hydrogen delivery to miniature PEM fuel cells has been the subject of considerable research activity in recent years [10–19].

2. The radial microreactor

In this paper, we present a novel radial flow micro packed bed *reactor-on-a-chip* with an integrated micro-vaporizer for hydrogen delivery using methanol reforming:

$$CH_3OH + H_2O \rightleftharpoons CO_2 + 3H_2 \quad (1)$$

* Corresponding author. Tel.: +1 610 758 6654; fax: 1 610 758 5057.
E-mail addresses: ashishpattekar@gmail.com (A.V. Pattekar), mayuresh.kothare@lehigh.edu (M.V. Kothare).

0378-7753/$ – see front matter © 2005 Elsevier B.V. All rights reserved.
doi:10.1016/j.jpowsour.2005.01.024

$$CH_3OH \rightleftharpoons CO + 2H_2 \quad (2)$$

$$CO + H_2O \rightleftharpoons CO_2 + H_2. \quad (3)$$

We have previously demonstrated rectangular microchannel based packed-bed microreactors for this application [19] as part of our ongoing work on this subject. The packing of microchannels (400 μm × 1000 μm) with catalyst particles of mean diameter 50–70 μm resulted in highly efficient contacting of reactants with the catalyst and excellent conversions at relatively low temperatures in the range of 195–210 °C. However, the inlet pressure of the methanol–water mixture required to drive the flow and generate sufficient hydrogen for an 8–10 W fuel cell was routinely found to be in the range of 70–100 psig in these conventional microchannel reactors. Such high inlet pressures are neither achievable nor desirable in portable devices nor can they be controlled using available miniature pumping devices and valves [20,21]. For true high energy density portable operation, the microreactor design should, therefore, be able to operate at significantly lower pressure drops while maintaining the high throughput rate for hydrogen production. The unique radial design presented here achieves this goal by exploiting several key characteristics of the methanol reforming reaction as discussed below.

An analysis of the different physical and chemical phenomena occurring inside the microchannel reactor reveals the inadequacy of simple microchannel based designs for practical micro-packed bed applications. The methanol reforming reaction causes an increase in the total number of moles of the reaction mixture, leading to an increase in gas mixture volume at a given pressure. This results in an increase in the gas flow velocity towards the outlet of the microchannels where a significant amount of methanol has already been converted to hydrogen. At the same time, the pressure decreases as the gas moves closer to the outlet due to the presence of a pressure gradient which drives the flow and this causes a further increase in the gas volumetric flow rate and gas flow velocity [19]. The result of both these effects is that higher velocity in local regions closer to the outlet leads to a smaller residence time in these regions, resulting in lower catalyst utilization. Also, since the bulk of the pressure drop in the microchannels occurs in the high gas velocity regions, such a design leads to high pressure drops in the device during operation, as was experimentally observed.

Vaporization of liquid feed in a microreactor also poses unique challenges due to the sudden expansion of the fluid during boiling which causes flow pulsation and *severe pressure drop oscillation* [22] in the two-phase flow region. This pulsation in the vaporization region leads to unsteady operation and the possibility of damage to the device unless sufficient room is provided for the nearly thousandfold expansion of the fluid as it changes from liquid to vapor.

All of the above problems have been resolved by employing a radial flow microreactor geometry which compensates for the expected gas expansion by providing a variable (increasing) flow cross section along the reaction path. As shown in Fig. 1(a), the reacting gases flow radially outward from the smaller inner circular boundary to the larger outer circular boundary, resulting in significantly reduced pressure drops compared to conventional microchannel based designs for a given feed flow rate. While radial flow reactors have been used in conventional chemical plants in the past [23], their use has been limited due to the more complex manufacturing process involved in implementing these designs at the macro scale. This is not an issue in micro scale radial reactors, since

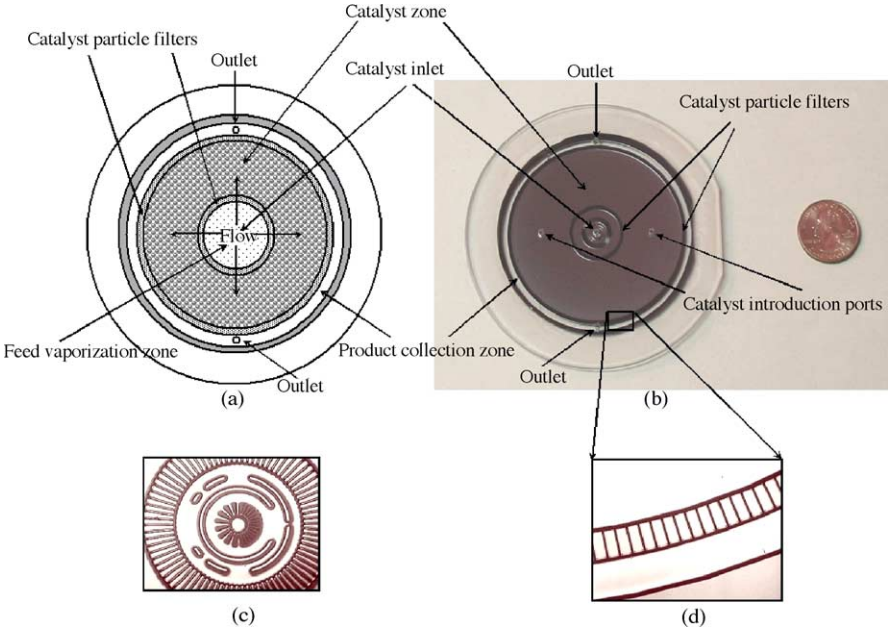

Fig. 1. Radial flow microreactor: (a) schematic; (b) fabricated device; (c) vaporization region; and (d) catalyst particle filter (*patent pending*).

the microfabrication steps involved are not much different for the radial and microchannel configurations.

Apart from the lower pressure drops, the radial design results in a very compact device, since a significantly larger amount of catalyst can be accommodated in a reactor of given volume compared to a microchannel based design in which the reactor walls take up a significant portion of the net reactor volume [19]. While this may not always be an important issue in conventional chemical plants which are typically the size of large buildings, compactness of design is of prime importance in portable devices where any increase in device size may severely limit its applicability. Thus, the radial microreactor exploits the unique advantages of the radial design at micro-scale, making the device especially well suited for plant-on-a-chip applications where low pressure drop and compactness of design are of prime importance.

3. Fabrication procedure

A schematic of the steps followed in fabricating the radial microreactor are given in Fig. 2. Standard photolithography steps followed by deep-reactive ion etching (DRIE) are used for etching features on a silicon substrate to form the vaporizer and filters for trapping catalyst particles. This is followed by anodic bonding to a pyrex wafer having drilled holes for catalyst introduction (two catalyst introduction ports) and microfluidic interfacing (one inlet and two symmetrically located outlets as shown in Fig. 1(b)). The procedure for carrying out the microfluidic interfacing is described elsewhere [24]. Finally, the catalyst is introduced into the annular reaction chamber by carrying out fluidized packing of $Cu/ZnO/Al_2O_3$ microparticles (*Süd-Chemie* catalyst C18-7) of diameters in the range of 50–70 μm. The catalyst powder is placed on the catalyst introduction ports and the inlet/outlet ports of the microreactor are connected to vacuum. This draws the microparticles into the reaction chamber where they are trapped in the annular region between the catalyst particle filters to form the radial packed bed shown in Fig. 2(e). The fabricated device along with magnified views of the different features is shown in Fig. 1(b)–(d).

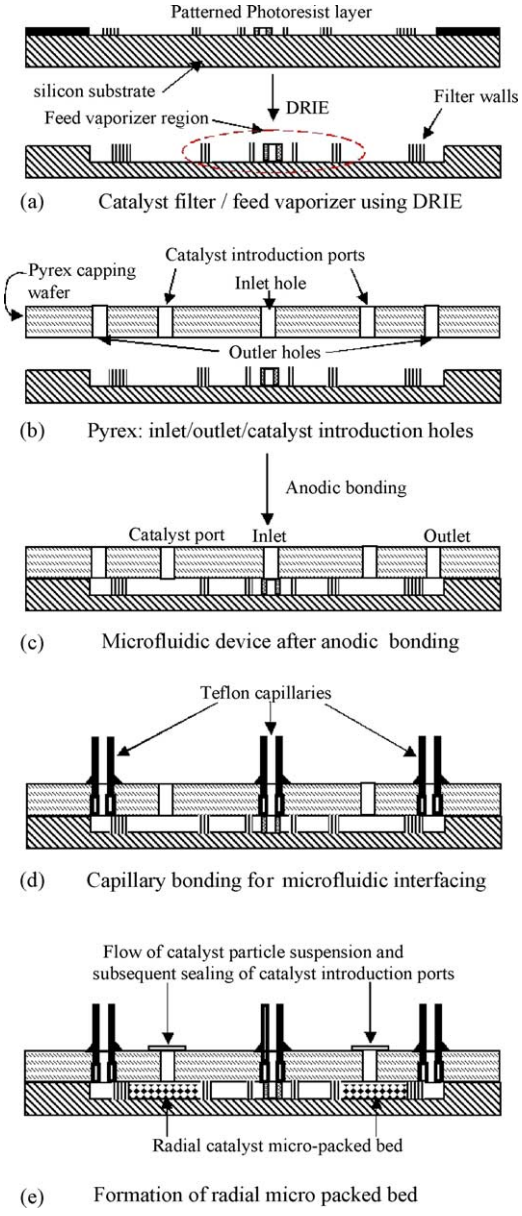

Fig. 2. Schematic of the steps followed in the fabrication of the radial microreactor.

4. Experimental verification

4.1. Experimental set-up

A schematic of the experimental set-up used for testing the microreactor is shown in Fig. 3 and the actual set-up is shown in Fig. 4. It consists of a syringe pump for feeding the liquid methanol–water mixture of required composition to the microreactor at desired flow rates and a mass spectrometer (Stanford Research Systems QMS-200 gas analyzer) which provides an on-line analysis of the composition of the reacted gases from the microreactor exit. An inert gas (argon) of known flow rate maintained using a mass flow controller is mixed with the microreactor exhaust gases before feeding into the gas analyzer. This provides for calculation of the exact hydrogen production rate by measuring the concentration of hydrogen relative to argon. A pressure sensor connected between the syringe pump and the microreactor inlet is used to monitor the pressure of the methanol–water mixture entering the microreactor.

The mass spectrometer takes in the desired amount of gas for analysis and the rest is either vented through a vacuum pump connected to the outlet side (Fig. 3) or collected in a sample balloon as shown in Fig. 4. The temperature of the microreactor is maintained at desired levels using a hotplate on which the microreactor is placed. As demonstrated previ-

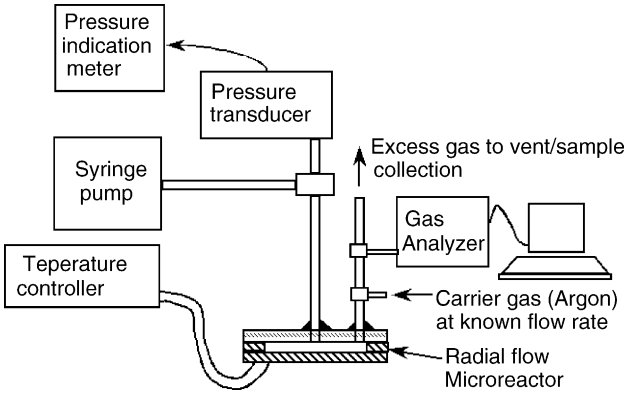

Fig. 3. Schematic of experimental setup.

ously [19], it is also possible to use on-chip heaters and temperature sensors for maintaining the operating temperature of the microreactor (Fig. 3) to avoid the use of bulky external hotplates and simplify the experimental set-up.

4.2. Pressure drop experiments

It was experimentally verified that this device could be operated at less than $\frac{1}{6}$th the pressure drops *and* with throughputs up to three times those possible using a microchannel configuration of the same overall reactor size, as shown in Fig. 5.

4.3. Vaporization experiments

The radial geometry of the design provides for expansion of the evaporating liquid radially outward from the inlet at the center and successfully dampens the pulsation effect discussed earlier. Special features were incorporated in the device as shown in Fig. 1(c) to provide sufficient area of contact between the liquid feed and the heated silicon surface to ensure proper vaporization. The central radial micro-walls in Fig. 1(c) serve as the initial point of contact for the liquid feed entering at the center. Subsequently, the two-phase fluid mixture meanders around the concentric walls and passes on to the catalyst packed reaction zone through another set of parallel walls providing further area for vaporization of the

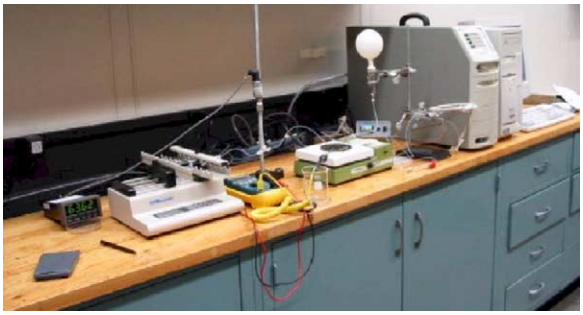

Fig. 4. The experimental setup.

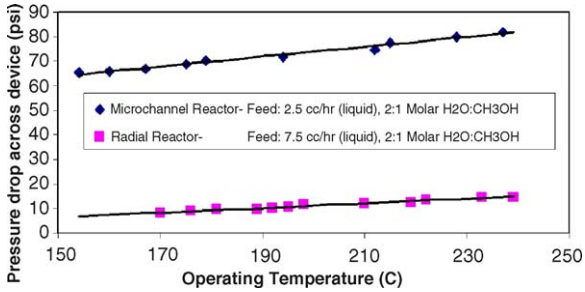

Fig. 5. Comparison of pressure drops in the microchannel device with pressure drops in the radial device at *three times* the throughput rate (feed: 2:1 molar H_2O:CH_3OH).

liquid feed. Though the presence of the meandering circular walls causes the feed to move in non-radial directions within the vaporization region, the features are arranged such that the fluid exits the vaporization region uniformly in all directions. This was verified by feeding liquid water at room temperature at the inlet and noting that the flow out of the vaporization zone was uniform in all directions [25].

The feed vaporization ability of the device was tested separately prior to carrying out the reaction runs by feeding liquid water at various flow rates and temperatures [26–28] and noting the maximum flow rate up to which the entire feed could be vaporized within the vaporization region. The device was able to successfully vaporize up to 15–25 $cm^3\,h^{-1}$ of liquid water feed at operating temperatures in the range of 150–200 °C without any liquid droplets appearing in the catalyst region, as shown in the vaporization runs. Snapshots from one of the vaporization runs at 200 °C [28] and water feed flow rates of 15 and 20 $cm^3\,h^{-1}$ are shown in Fig. 6(a) and (b), respectively. Liquid droplets can be seen clearly within the vaporization region at the high 20 $cm^3\,h^{-1}$ flow rate, but all fluid entering the catalyst zone (marked by the outer circular boundary of the vaporizer shown in Fig. 6(a) and (b)) is in gaseous phase (note the absence of liquid droplets in this region), thus, verifying complete vaporization. Since the maximum flow rate of the methanol–water liquid feed during the subsequent reaction runs needed to produce hydrogen for a 20-W fuel cell was less than 10 $cm^3\,h^{-1}$, the vaporization capacity was demonstrated to be sufficient for the range of interest of the feed flow rates.

5. Results from reaction runs

Results from experimental reaction runs of the radial reactor are shown in Table 1 and in Fig. 7. The temperature of the microreactor was varied in the range of 150 to about 250 °C for different feed flow rates and feed compositions. The hydrogen production rate for each run rises as increasing the reactor operating temperature results in faster kinetics to the point when equilibrium conversions are reached and no further increase in hydrogen production rate is possible. Since the methanol reforming reaction can proceed to almost complete conversion at equilibrium under the operating con-

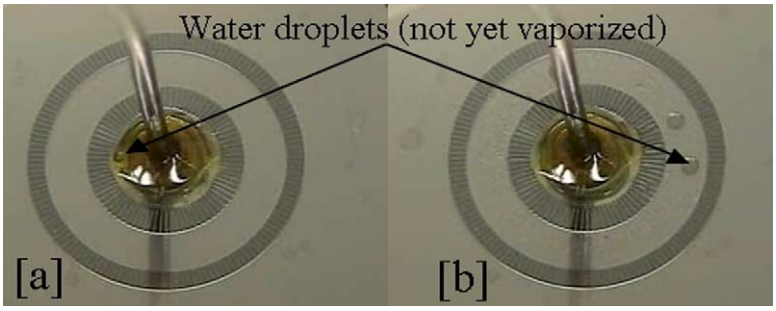

Fig. 6. Vaporizer operation at 200 °C: (a) water feed 15 $cm^3\,h^{-1}$; (b) water feed 20 $cm^3\,h^{-1}$.

ditions studied here [29], this represents close to complete conversion of methanol in the radial reactor. The conversion values were calculated using the data reported in the table and were found to be higher than 98% for each of the reaction runs. As shown in Table 1, higher water to methanol ratios in the feed lead to an increase in the number of moles of hydrogen produced per mole of methanol in the feed due to the suppression of carbon monoxide production via reaction (3) above.

The peak hydrogen production rate achieved with the radial device was about 145 SCCM (sufficient for a 20 W fuel cell), as shown in Fig. 7. The pressure drop across the device at this peak production rate was found to be 10.2 psi. In contrast, the microchannel device developed earlier [19] provided a peak hydrogen production rate of 72 SCCM, at a pressure drop exceeding 95 psi. Thus, it was experimentally verified that the radial device can produce more than twice the amount of hydrogen compared to the microchannel device, at less than $\frac{1}{9}$th of the pressure drop.

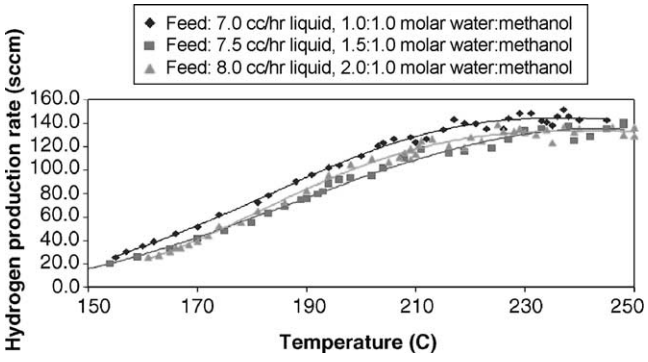

Fig. 7. Hydrogen production rate in radial microreactor at various temperatures and feeds.

6. Mathematical analysis

Rigorous mathematical modeling and analysis was carried out to understand the observed improvement in performance with the radial configuration in comparison to the microchannel configurations developed earlier. The main equations of the model are discussed below, followed by results from numerical integration of the developed models.

6.1. Coupled flow and reaction kinetics modeling

A comprehensive model based on coupled reaction kinetics and momentum transport equations is provided below. FORTRAN programs were developed to integrate the model equations numerically using the method of lines. As discussed below, the simulation results support the experimentally observed behavior (significantly lower pressure drops at *higher* throughputs in the radial device compared to the microchannel device) and serve as further verification of the advantage of the radial geometry for high throughput, low pressure drop applications.

Darcy's law for flow through porous media (Eq. (4)) [30] and the continuity equation for compressible fluids (Eq. (5)) [31] are used to model gas flow through the micro-packed bed, where $\boldsymbol{u}$ is the fluid flow velocity vector; K_p, the permeability of the porous medium; P denotes the pressure; μ denotes the fluid viscosity and ρ, the fluid density:

$$\boldsymbol{u} = u_x\boldsymbol{i} + u_y\boldsymbol{j} + u_z\boldsymbol{k} = -\frac{K_p}{\mu}\nabla P \tag{4}$$

$$\nabla \cdot (\rho \times \boldsymbol{u}) = 0 \tag{5}$$

The gas is modeled as a compressible fluid in accordance with the ideal gas law:

$$PV = nRT \tag{6}$$

Table 1
Results from experimental operation of the radial microreactor

Feed composition (molar H_2O:CH_3OH)	Feed flow rate (liquid, 20 °C) ($cm^3\,h^{-1}$)	Moles of H_2 produced per mole CH_3OH feed	Mol% CO in product
1:1	7.0	2.83	3.13
1.5:1	7.5	2.85	2.52
2:1	8.0	2.96	2.18

where V denotes the volume occupied by n moles of the gas at temperature T and R is the universal gas constant. This can also be written as

$$\frac{nM}{V} = \rho = \frac{MP}{RT} \tag{7}$$

where M denotes the gas molecular weight. Eqs. (4), (5) and (7) can be combined into a single governing equation describing the flow of the gas mixture through the packed bed of catalyst particles:

$$\nabla \cdot \left(-\frac{K_p M}{\mu RT} P \nabla P \right) = 0 \tag{8}$$

and since K_p and R are constants and assuming that T is maintained constant across the reactor geometry by proper temperature control, this becomes:

$$\nabla \cdot \left(-\frac{M}{\mu} P \nabla P \right) = 0. \tag{9}$$

Considering variations only in radial direction (axisymmetry), we have:

$$\frac{1}{r}\frac{\partial}{\partial r}\left(r \frac{MP}{\mu}\frac{\partial P}{\partial r} \right) = 0 \tag{10}$$

$$\Rightarrow \frac{\partial}{\partial r}\left(r \frac{MP}{\mu}\frac{\partial P}{\partial r} \right) = 0 \tag{11}$$

$$\Rightarrow \frac{rMP}{\mu}\frac{\partial^2 P}{\partial r^2} + \frac{rM}{\mu}\left(\frac{\partial P}{\partial r}\right)^2 + \frac{rP}{\mu}\frac{\partial P}{\partial r}\frac{\partial M}{\partial r} + \frac{MP}{\mu}\frac{\partial P}{\partial r} - \frac{rMP}{\mu^2}\frac{\partial P}{\partial r}\frac{\partial \mu}{\partial r} = 0. \tag{12}$$

Then using the notation

$$\left(\frac{\partial P}{\partial r}\right) = m \tag{13}$$

and removing the partial derivative sign for this one-dimensional (radial) representation, we have from Eqs. (12) and (13) above,

$$\left(\frac{\mathrm{d}m}{\mathrm{d}r}\right) = -\frac{m^2}{P} - \frac{m}{r} - \frac{m}{M}\frac{\mathrm{d}M}{\mathrm{d}r} + \frac{m}{\mu}\frac{\mathrm{d}\mu}{\mathrm{d}r}. \tag{14}$$

Eqs. (13) and (14) constitute the fluid mechanics model for the radial reactor. In this model, the effect of reaction is captured through variations in effective molecular weight 'M' and viscosity 'μ' of the reacting mixture. For the methanol reforming system,

$$CH_3OH + H_2O \rightleftharpoons CO_2 + 3H_2 \tag{15}$$

$$CH_3OH \rightleftharpoons CO + 2H_2 \tag{16}$$

$$CO + H_2O \rightleftharpoons CO_2 + H_2 \tag{17}$$

denoting the forward rate of the reactions (mol m^{-3} s^{-1}) given in Eqs. (15)–(17) above by r_1, r_2, and r_3, respectively the rate of *production* of each species is given by:

$$r_{CH_3OH} = -r_1 - r_2 \tag{18}$$

$$r_{H_2O} = -r_1 - r_3 \tag{19}$$

$$r_{CO_2} = r_1 + r_3 \tag{20}$$

$$r_{H_2} = 3r_1 + 2r_2 + r_3 \tag{21}$$

$$r_{CO} = r_2 - r_3 \tag{22}$$

The rates r_1, r_2 and r_3 are functions of the partial pressures (P_j, N m^{-2}) of the different species in the reacting mixture, which are given by:

$$P_j = n_j \times P \tag{23}$$

where P is the total pressure (N m^{-2}) and n_j is the mole fraction of each species, given by:

$$n_j = \frac{F_j}{F_T} \tag{24}$$

where 'j' represents any of CH_3OH, H_2O, CO_2, CO and H_2 and F is the flow rate in mol s^{-1}. This is in turn used to calculate the molecular weight M for use in Eq. 14 via the equation:

$$M = \sum_{j=1}^{n} n_j M_j. \tag{25}$$

Also, the effect of variation in viscosity of the reaction mixture as its composition changes with reaction is included in Eq. (14) above. The mixture viscosity (μ), which is a function of the temperature (T), pressure (P), and composition (n_j), is calculated during the numerical solution by using correlations and mixing rules available in the literature [32].

In order to incorporate the effect of chemical reactions in the above fluid dynamics model, we write the following balance for the flow rate F_j (mol s^{-1}) of each species in the radial flow device:

$$\frac{\mathrm{d}F_j}{\mathrm{d}V} = \frac{\mathrm{d}F_j}{2\pi r h\,\mathrm{d}r} = r_j\,(\mathrm{mol}\,(\mathrm{m}^{-3}\,\mathrm{s}^{-1})) \tag{26}$$

$$\Rightarrow \left(\frac{\mathrm{d}F_j}{\mathrm{d}r}\right) = (2\pi r h) r_j \tag{27}$$

where 'h' is the thickness of the radial catalyst packed bed and 'r_j' represents the rate of production of each species, given in Eqs. (18)–(22) above.

Eqs. (13), (14) and (27) represent the complete coupled model for fluid flow and reactions in the radial microreactor, which can be solved using a numerical integration technique, such as the method of lines.

A similar analysis for the microchannel design (analyzing a single reactor microchannel) gives the following model for the tubular configuration, with 'z' representing the distance

Table 2
Parameters used in the simulation—constants

$C^T_{S_1} = 7.5 \times 10^{-6}\ \text{mol m}^{-2}$	$S_c = 102\ \text{m}^2\ \text{g}^{-1}$
$C^T_{S_{1a}} = 1.5 \times 10^{-5}\ \text{mol m}^{-2}$	$\rho_b = 1300\ \text{kg m}^{-3}$
$C^T_{S_2} = 7.5 \times 10^{-6}\ \text{mol m}^{-2}$	$R = 8.314\ \text{J (mol K)}^{-1}$
$C^T_{S_{2a}} = 1.5 \times 10^{-5}\ \text{mol m}^{-2}$	$T = 245\ ^\circ\text{C} = 518.15\ \text{K}$

Table 3
Parameters used in the simulation—k and K parameter values calculated at the reforming temperature of 245 °C = 518 K

$k_R = 31813.7\ \text{m}^2\ (\text{mol s})^{-1}$	$K^*_{\text{HCOO}(1)} = 0.18902\ \text{bar}^{-1.5}$
$k_W = 86502.8\ \text{m}^2\ (\text{mol s})^{-1}$	$K_{H(1a)} = 0.59799\ \text{bar}^{-1}$
$k_D = 2732.26\ \text{m}^2\ (\text{mol s})^{-1}$	$K_{H(2a)} = 425.41\ \text{bar}^{-1}$
$K^*_{\text{CH}_3\text{O}(1)} = 0.68135\ \text{bar}^{-0.5}$	$K^*_{\text{CH}_3\text{O}(2)} = 3836.6\ \text{bar}^{-0.5}$
$K^*_{\text{OH}(1)} = 0.49241\ \text{bar}^{-0.5}$	$K^*_{\text{OH}(2)} = 3836.6\ \text{bar}^{-0.5}$

along the reaction channel and 'w' and 't' representing the microchannel width and thickness, respectively:

$$\left(\frac{\mathrm{d}P}{\mathrm{d}z}\right) = m \tag{28}$$

$$\left(\frac{\mathrm{d}m}{\mathrm{d}z}\right) = -\frac{m^2}{P} - \frac{m}{M}\frac{\mathrm{d}M}{\mathrm{d}z} + \frac{m}{\mu}\frac{\mathrm{d}\mu}{\mathrm{d}z} \tag{29}$$

$$\left(\frac{\mathrm{d}F_j}{\mathrm{d}z}\right) = (wt)r_j. \tag{30}$$

In order to compute the reaction rates r_1 , r_2 and r_3, the comprehensive kinetic model developed by Peppley et al. [33] was implemented in the simulations. The main equations of this model are given in Eqs. (31)–(33) below and the various parameters used in the model are listed in Tables 2 and 3.

All temperature-dependent 'k' and 'K' values listed in Table 3 are calculated at the reforming temperature of 245 °C, based on formulae available in [33].

$$r_1 = \frac{k_R K^*_{\text{CH}_3\text{O}(1)} \left(P_{\text{CH}_3\text{OH}}/P^{0.5}_{\text{H}_2}\right)\left(1 - P^3_{\text{H}_2}P_{\text{CO}_2}/k_R P_{\text{CH}_3\text{OH}}P_{\text{H}_2\text{O}}\right) C^T_{S_1} C^T_{S_{1a}} S_c \rho_b}{\left(1 + K^*_{\text{CH}_3\text{O}(1)}\left(P_{\text{CH}_3\text{OH}}/P^{0.5}_{\text{H}_2}\right) + K^*_{\text{HCOO}(1)}P_{\text{CO}_2}P^{0.5}_{\text{H}_2} + K^*_{\text{OH}(1)}\left(P_{\text{H}_2\text{O}}/P^{0.5}_{\text{H}_2}\right)\right)\left(1 + K^{0.5}_{H(1a)}P^{0.5}_{\text{H}_2}\right)} \tag{31}$$

$$r_1 = \frac{k^*_W K^*_{\text{OH}(1)}(P_{\text{CO}}P_{\text{H}_2\text{O}}/P^{0.5}_{\text{H}_2})(1 - P_{\text{H}_2}P_{\text{CO}_2}/k_W P_{\text{CO}}P_{\text{H}_2\text{O}})(C^T_{S_1})^2 S_c \rho_b}{(1 + K^*_{\text{CH}_3\text{O}(1)}\left(P_{\text{CH}_3\text{OH}}/P^{0.5}_{\text{H}_2}\right) + K^*_{\text{HCOO}(1)}P_{\text{CO}_2}P^{0.5}_{\text{H}_2} + K^*_{\text{OH}(1)}(P_{\text{H}_2\text{O}}/P^{0.5}_{\text{H}_2}))^2} \tag{32}$$

$$r_3 = \frac{k_D K^*_{\text{CH}_3\text{O}(2)}\left(P_{\text{CH}_3\text{OH}}/P^{0.5}_{\text{H}_2}\right)(1 - P^2_{\text{H}_2}P_{\text{CO}}/k_D P_{\text{CH}_3\text{OH}}) C^T_{S_2} C^T_{S_{2a}} S_c \rho_b}{(1 + K^*_{\text{CH}_3\text{O}(2)}(P_{\text{CH}_3\text{OH}}/P^{0.5}_{\text{H}_2}) + K^*_{\text{OH}(2)}(P_{\text{H}_2\text{O}}/P^{0.5}_{\text{H}_2}))(1 + K^{0.5}_{H(2a)}P^{0.5}_{\text{H}_2})} \tag{33}$$

where $C^T_{S_1}$, $C^T_{S_{1a}}$, $C^T_{S_2}$ and $C^T_{S_{2a}}$ are the concentrations of active sites on the catalyst surface, S_c is specific surface area and ρ_b is catalyst bulk density, respectively [33].

6.2. Simulation results

The results from the numerical integration of the above models for the radial and microchannel device are given in Figs. 8 and 9. It is clear that for the same overall reactor size, the radial design provides twice the hydrogen production rate of the microchannel design, at a fraction of the pressure drop. The radial device fabricated in this work had an overall size (net reactor volume) comparable to a previously fabricated microchannel based design [19] with seven parallel microchannels, each microchannel of dimensions 400 μm × 1000 μm × 10.4 cm. Thus, in order to make a fair comparison of the expected pressure drops, the flow rate used in the simulation of a single microchannel was appropriately scaled to $\frac{1}{7}$th of the total feed into the microchannel device.

As seen in Fig. 8(a), for a methanol + water feed flow rate sufficient to generate enough hydrogen for a *10-W fuel cell*, the pressure drop across the microchannel device was found to be about 7.8 atm. In contrast, the pressure drop across the radial device was found to be about 0.7 atm for a methanol + water feed flow rate sufficient to generate enough hydrogen for a *20-W fuel cell* (see Fig. 9(a)).

As seen in Fig. 8(b), the tubular (microchannel) device has a steep rise in the flow velocity near the exit due to the increase in the number of moles during the reaction and expansion of the reacting mixture, which leads to non-uniform catalyst utilization in this region and high pressure drop during the operation. These effects are successfully countered in the radial geometry and there is a significantly lower variation in the flow velocity magnitude in the radial device compared to the microchannel device as seen in Figs. 9(b) and 8(b), leading to a more uniform catalyst utilization and significantly lower pressure drop in the radial device. Thus, the simulation results support the experimental observations regarding the higher throughput capacity of the radial device with operation at a fraction of the overall pressure drop, as noted in Section 5 above.

It must be noted that the main objective of the simulations was to demonstrate the advantage of the radial geometry in providing a significant reduction in the operating pressure drops. To that end, any kinetic model which reasonably represents the reforming process would have been adequate. The comprehensive kinetic model [33] used in this work is considered to be the most general form, and was, therefore, chosen for the simulation studies to verify the hypotheses regarding the advantages of the radial microreactor configuration.

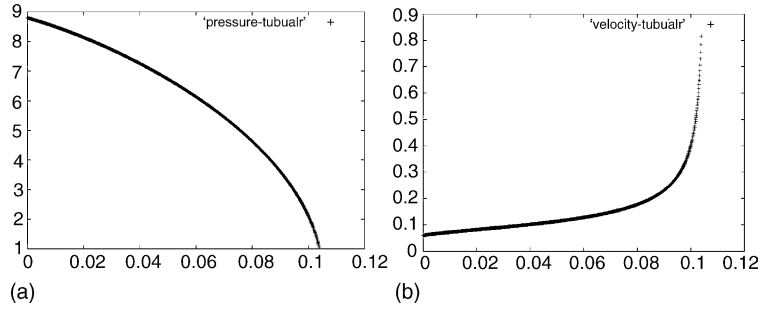

Fig. 8. (a) Pressure profile in microchannel reactor—fluid pressure (atm) vs. distance along the microchannel (m); (b) velocity profile in microchannel reactor—fluid velocity (m/s) vs. distance along the microchannel (m) (at a hydrogen production rate sufficient for a 10-W fuel cell).

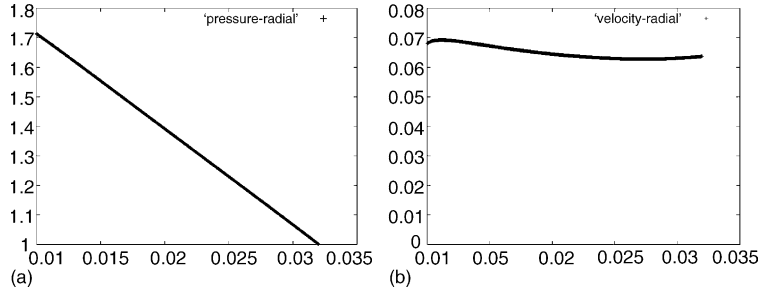

Fig. 9. (a) Pressure profile in radial reactor—fluid pressure (atm) vs. distance from device center (m); (b) velocity profile in radial reactor—fluid velocity (m/s) vs. distance from device center (m) (at a hydrogen production rate sufficient for a 20-W fuel cell).

7. Energy density calculations and comparisons

We will now proceed to calculate the projected energy storage capacities possible using the integrated system consisting of the radial microreformer coupled with a micro fuel cell and to draw out important conclusions regarding the viability of this technology in comparison with current state of the art batteries.

7.1. The need for alternative portable power sources

Kelley et al. [34] and have provided a comparison of the specific energy density (φ, Watt–hour energy storage per kg weight of the battery system) possible using current state of the art miniature power sources (summarized in Table 4). Considering the projected improvements in the lithium-ion battery [35], it can be expected that the energy storage capacity of commercially available rechargeable batteries may be improved up to about 450 Wh l^{-1} or about 275 Wh kg^{-1} over the next few years [35]. In contrast, based on the DARPA palm power initiative guidelines [36], it is clear that several key applications exist for portable energy storage systems with capacities in the range of 1000 Wh kg^{-1} (20 W, 3-h mission) to over 3000 Wh kg^{-1} (20 W, 10-day mission). Thus, a new micro-power technology may be the only alternative if these higher energy densities are to be attained for portable power.

7.2. PEM fuel cell specifications

For a typical PEM fuel cell operating at 60% thermal efficiency, a hydrogen flow rate of 0.42 g mol h^{-1} would be needed for 20 W operation [37]. Thus, a 20 h continuous operation at 20 W would require 8.40 g mol of H_2. This translates into a net methanol storage requirement of 2.947 g mol, or 94.32 g methanol, assuming 2.85 mol H_2 produced per mol CH_3OH feed to the reformer as per Table 1, for a feed ratio of 1.5:1 molar H_2O:CH_3OH. Now, a 1.5:1 molar H_2O:CH_3OH mixture has a density of 0.9067 g/cm^3 at 20 °C and contains 0.49225 g methanol per cc of the mixture [32]. Thus, the net water-methanol (1.5:1 molar) feed mixture storage requirement for a 20 W, 20 h operation would, therefore, be 173.73 g, or 191.61 cm^3.

Based on the microfabricated fuel cell sizes reported by Kelley et al. [34], a typical micro fuel cell for 20 W application (basis: μFC mass 0.031 g, volume 0.012 cm^3, with an active area of 0.25 cm^2, operating at a power density of 80 mW cm^{-2}) would have a mass of $0.031 \times 20/(0.08 \times 0.25) = 31$ g and a volume of 12 cm^3. Also, the reformer reported in this work, when scaled for the above application (hydrogen supply for a 20 W fuel cell = 0.42 g mol h^{-1} H_2 production rate) would have a mass of about 35 g including the packaging for thermal insulation, and a volume of about 28 cm^3. Thus, the reformer–fuel cell combination would have

Table 4
Specific energy density of current state of the art miniature power sources

Battery type	Specific energy (Wh kg^{-1})
Ni/Cd battery	60
Ni/metal hydride battery	65
$Li/Li_xMn_2O_4$ battery	130
LiC_6/Li_xCoO_2 battery	90

Table 5
Energy requirement for operation of microreformer producing hydrogen for a 20 W fuel cell

Reformer process step	Energy requirement (W)
Sensible heating of water in feed	0.6954
Sensible heating of methanol in feed	0.5504
Vaporization requirement for water	2.4483
Vaporization requirement for methanol	1.3942
Endothermic heat of reaction	2.3850
Total power required for operation	7.4733

an intrinsic mass of 66 g and a volume of about 40 cm^3, in addition to the storage requirements for methanol and water discussed above. This makes the total mass and volume of the power source (system + fuel) equal to about $(66 + 174) = 240$ g and $(40 + 192) = 232\ cm^3$, respectively.

7.3. Reformer energy requirement

To make a fair comparison between miniature fuel cells and state of the art miniature batteries, not only does one need to consider a basis related to the type of application being evaluated and the volume and weight of the energy conversion devices involved, but also the overall energy requirement for operating the power source (e.g., liquid feed vaporization and endothermic reforming reaction heat requirements, heat loss to the ambient, and overall fuel cell efficiency, etc. in the case of the microreformer-micro fuel cell combination). A detailed analysis of the the energy requirement of each of the process steps carried out in the microreformer is provided in Appendix A and summarized in Table 5. As shown, a reformer providing sufficient hydrogen for a 20 W fuel cell application would require about 7.4733 W power to vaporize the liquid fuel/water mixture and carry out the reforming reaction.

7.4. Projected energy storage density

Assuming absolutely no thermal integration between the reformer and the fuel cell, if the entire reformer energy requirement is satisfied by electricity produced in the fuel cell, this translates into a useful energy storage capacity of $20\,h \times (20 - 7.4733)\,W = 250.534$ Wh.

Going back to the 20 W, 20 h basis, the total mass and volume of the power source (fuel + system) are 240 g and 232 cm^3, respectively. This translates into an energy storage capacity of 1044 Wh kg^{-1} and 1080 Wh l^{-1} for this system. Of course, this calculation does not consider the energy requirement for pumping the fuel/water mixture at inlet pressure, the heat loss to the surrounding during the operation and the efficiency of the power conditioning circuits that are typically necessary in fuel cell based power supplies, which would potentially bring down the above values by as much as 25%, to about 783 Wh kg^{-1} and about 810 Wh l^{-1}. However, there is also no allowance for heat integration between the fuel cell and the reformer, which could increase the overall system efficiency and the energy storage density by a significant amount. For example, a 72% H_2 utilization in the fuel cell would result in useful electrical energy output from the fuel cell equal to $(20\,W \times 20\,h \times 0.72) = 288$ Wh, with a hydrogen flow rate of 0.1176 mol h^{-1} in the fuel cell anode off-gas (effluent). If the heating requirement for the reformer operation is supplied by combustion of the un-utilized hydrogen in the anode off-gas, this translates into a heating capacity of 7.8302 W based on the lower heating value (LHV) of hydrogen, which is more than sufficient to provide the reformer requirement of 7.4733 W given in Table 5. This system would then have an overall energy storage density of 1200 Wh kg^{-1}, or about 1241 Wh l^{-1}.

Recent developments in high temperature PEM fuel cells have led to novel membranes that can operate at high temperatures, up to 200 °C [38]. High temperature PEM fuel cells offer several advantages, including simpler water management and high CO tolerance (up to about 2% CO in the fuel), which significantly reduces the amount of post-reforming fuel clean-up steps required. With proper control of the reforming conditions to maintain levels below 2%, CO clean-up can be completely avoided, significantly simplifying the overall system. Apart from this, another important advantage of the high temperature PEM fuel cell is that the waste heat is available for exchange at a higher temperature, resulting in the possibility of further heat integration in the overall system. For example, continuing the above analysis, 40% of the thermal energy in the hydrogen used in the fuel cell is wasted as heat (60% thermal efficiency). This translates into net heat energy of $[0.42\,mol\,h^{-1} \times 0.72$ (fuel utilization) $\times\ 0.40 \times 239700.0\,J\,mol^{-1}$(LHV of H_2)$]/3600(s\,h^{-1}) = 8.054$ W at 200 °C available for further integration into the system and also to take care of the heat loss, providing a further improvement in the energy storage density. Including a 15% penalty for the energy requirement related to fluid pumping and power conditioning losses, this makes the overall energy storage densities of $1200 \times 0.85 = 1020$ Wh kg^{-1}, or $1241 \times 0.85 = 1055$ Wh l^{-1} easily attainable in a practical system.

Water produced in the fuel cell may be recycled into the system to satisfy the reformer requirement, further improving the overall efficiency and energy storage capacity of the system. For example, in a fuel cell operating at 80% fuel utilization, the effluent is steam at 200 °C at a flow rate of $(0.42 \times 0.80) = 0.336$ g mol h^{-1}. Noting that the steam required in the reformer is $1.5 \times (0.42/2.85) = 0.2211$ g mol h^{-1}, the steam requirement in the reformer may be completely satisfied through the fuel cell effluent if proper flow separation and control systems are implemented. Such a highly integrated system will also require significantly lower energy for operating the reformer, since the heating requirements for the water feed are satisfied directly through the waste heat in the fuel cell. For the 20 W, 20 h basis, the net volume and weight of the fuel cartridge would then be 94.32 g, or about 121 cm^3 (pure methanol). Assuming a slightly larger fuel cell + reformer system (80 g, 55 cm^3) for incorporating the integration

mechanism, the net size of fuel + system in this case would be 174.32 g and 176 cm^3. The net reformer energy requirement would be about 4.4268 W (since steam at 200 °C is available from the fuel cell). The hydrogen flow in the anode off-gas would be $0.42 \times 0.20 = 0.084\,mol\,h^{-1}$, representing a heating capacity of 5.593 W, which is more than enough to satisfy the reformer energy requirement. The energy storage capacity of this highly integrated system would then be $(20\,W \times 20\,h \times 0.80) = 320$ Wh. Again, including a 15% penalty for the energy requirement related to fluid pumping and power conditioning losses, this translates into an energy storage density of 1560 $Wh\,kg^{-1}$ or about 1545 $Wh\,l^{-1}$, a five- to six-fold improvement compared to the best state of the art rechargeable batteries available today. Longer run times result in higher energy storage capacity, since the ratio of the storage volume and weight of the fuel to the system would increase. For a three-day run, this translates into a stored energy of $(20\,W \times 72\,h \times 0.80) = 1152$ Wh, with a net storage weight and volume of $(339.55 + 80)$ g and $(435.6 + 55)\,cm^3$, respectively. With the 15% penalty for system losses, this would make the energy storage density for a 3-day run to be 2334 $Wh\,kg^{-1}$ or about 1996 $Wh\,l^{-1}$. For a 10-day (240 h) run, the energy density would be 2693 $Wh\,kg^{-1}$ or about 2167 $Wh\,l^{-1}$, thus, proving micro fuel cell technology to be a viable alternative for portable power needs of the future.

8. Conclusion

A completely novel approach to carrying out chemical reactions in a microreactor was presented in this paper. Conventional microchannel based designs were found to be inadequate for microreaction systems which involve increase in the moles due to reaction and corresponding expansion of the reaction mixture. The radial device presented here not only solves the problems associated with the microchannel geometry, but also it allows for rigorous modeling and analysis of the operation due to the simple geometry. Rigorous modeling and simulation studies of the device operation revealed the advantages of the new design and confirmed the reasoning behind adopting this approach for developing the microreactor. The developed microreactor produces sufficient hydrogen for fuel cells in the range of up to 20 W and thus opens the path for portable fuel cell based energy systems utilizing reforming technology for hydrogen delivery.

As the demand for high energy density power sources grows with the introduction of ever more power hungry multifunctional portable electronic devices, miniature fuel cells are likely to provide an excellent solution to the problems faced by the portable rechargeable batteries of today. Surely, several challenges need to be overcome before widespread introduction of this technology can be successful. Integration of the reformer and fuel cell system, balance of plant issues, efficient power conditioning systems, and reliability of long-term operation are just some of the issues that need to be resolved in a prototype power source utilizing this technology. As development continues and these problems are resolved, the microreformer – micro fuel cell combination with estimated energy storage densities in the range of up to 2693 $Wh\,kg^{-1}$ can definitely be expected to appear in the portable energy market of the future.

Acknowledgements

This work was supported in part by the U.S. National Science Foundation ("XYZ-on-a-Chip" initiative Grant CTS-9980781) and the Pittsburgh Digital Greenhouse. Fabrication of the microreactor was performed in part at the Cornell Nano-Scale Science and Technology Facility (a member of the National Nanofabrication Users Network) which is supported by the National Science Foundation under Grant ECS-9731293, its users, Cornell University and Industrial Affiliates. The authors would also like to acknowledge the help of J. Zelinski (Lehigh University's Physics Department Machine Shop) in the drilling of the pyrex wafers.

Appendix A

A detailed analysis of the energy requirement of each of the process steps carried out in the microreformer is provided in this appendix. The results of these calculations are summarized in Table 5.

A.1. Sensible heating of methanol

The vapor pressure of methanol is given by [39]:

$$\log_{10}(P^{sat}_{CH_3OH}) = 45.6171 - \frac{3.2447 \times 10^3}{T} - 13.988 \log_{10}(T) + 6.6365 \times 10^{-3} T - 1.0507 \times 10^{-13} T^2 \quad (A.1)$$

where $P^{sat}_{CH_3OH}$ is measured in mmHg and T is the absolute temperature. Thus, at the reformer inlet pressure of 1.7 atm (see Fig. 9(a)), the boiling point of CH_3OH is 351.85 K, obtained from the above equation.

The specific heat capacity of liquid methanol $C_p^{CH_3OH,(l)}$ $(J\,(mol\,K)^{-1})$ is given by [39]:

$$C_p^{CH_3OH,(l)} = 40.152 + 3.1046 \times 10^{-1} T - 1.0291 \times 10^{-3} T^2 + 1.4598 \times 10^{-6} T^3 \quad (A.2)$$

where T is the absolute temperature. Therefore, the sensible heat requirement for liquid methanol from a room temperature of 298.15 K to its boiling point of 351.85 K is:

$$\int_{298.15}^{351.85} C_p^{CH_3OH,(l)} dT = 4433.458\,J\,mol^{-1}. \quad (A.3)$$

Also, the specific heat capacity of methanol vapor $C_p^{CH_3OH,(g)}$ $(J\,(mol\,K)^{-1})$ is given by [39]:

$$C_p^{\mathrm{CH_3OH,(g)}} = 40.046 - 3.8287 \times 10^{-2}T + 2.4529 \times 10^{-4}T^2 - 2.1679 \times 10^{-7}T^3 + 5.99 \times 10^{-11}T^4. \quad (A.4)$$

Therefore, the sensible heat requirement for methanol vapor from its boiling point of 351.85 K to the reactor operating temperature of 245 °C = 518.15 K is:

$$\int_{351.85}^{518.15} C_p^{\mathrm{CH_3OH,(g)}} \mathrm{d}T = 9009.682\,\mathrm{J\,mol^{-1}}. \quad (A.5)$$

Thus, the total sensible heat load for methanol is:

$$\triangle H_{\mathrm{total}}^{\mathrm{CH_3OH,sensible}} = 13443.14\,\mathrm{J\,mol^{-1}}. \quad (A.6)$$

For a methanol flow rate of 0.1474 mol h^{-1} (sufficient to produce 0.1474 × 2.85 = 0.420 mol h^{-1} of H_2), this translates into an energy requirement of 13443.14 × 0.1474/3600 = 0.5504 W.

A.2. Methanol vaporization

The enthalpy of vaporization of methanol is given by [39]:

$$\triangle H_{\mathrm{CH_3OH}}^{v} = 52.723\left(1 - \frac{T}{512.58}\right)^{0.377}\mathrm{kJ\,mol^{-1}}. \quad (A.7)$$

Thus, the methanol vaporization heating requirement at the boiling temperature of 351.85 K is

$$52.723\left(1 - \frac{351.85}{512.58}\right)^{0.377}\mathrm{kJ\,mol^{-1}} \times \frac{0.1474}{3600}\,\mathrm{mol\,s^{-1}} = 1.3942\,\mathrm{W}. \quad (A.8)$$

A.3. Sensible heating of water

At the reactor feed pressure of 1.7 atm, the boiling point of water is 388.70 K, obtained from steam tables [32]. For calculating the liquid water heating requirement, we have the following correlation for specific heat capacity of water [39]:

$$C_p^{\mathrm{H_2O,(l)}} = 92.053 - 3.9953 \times 10^{-2}T - 2.1103 \times 10^{-4}T^2 + 5.3469 \times 10^{-7}T^3\,\mathrm{J\,(mol\,K)^{-1}} \quad (A.9)$$

Therefore, the sensible heat requirement for liquid water from a room temperature of 298.15 K to its boiling point of 388.70 K is:

$$\int_{298.15}^{388.70} C_p^{\mathrm{H_2O,(l)}} \mathrm{d}T = 6821.339\,\mathrm{J\,mol^{-1}}. \quad (A.10)$$

Also, the specific heat capacity of water vapor $C_p^{\mathrm{H_2O,(g)}}$ (J $(\mathrm{mol\,K})^{-1}$) is given by [39]:

$$C_p^{\mathrm{H_2O,(g)}} = 33.933 - 8.4186 \times 10^{-3}T + 2.9906 \times 10^{-5}T^2 - 1.7825 \times 10^{-8}T^3 + 3.6934 \times 10^{-12}T^4. \quad (A.11)$$

Therefore, the sensible heat requirement for steam from its boiling point of 388.70 K to the reactor operating temperature of 245 °C = 518.15 K is:

$$\int_{388.70}^{518.15} C_p^{\mathrm{H_2O,(g)}} \mathrm{d}T = 4501.367\,\mathrm{J\,mol^{-1}}. \quad (A.12)$$

Thus, the total sensible heat load for water is:

$$\triangle H_{\mathrm{total}}^{\mathrm{H_2O,sensible}} = 11322.71\,\mathrm{J\,mol^{-1}}. \quad (A.13)$$

For a water flow rate of 0.2211 mol h^{-1} (sufficient to produce (0.2211/1.5) × 2.85 = 0.420 mol h^{-1} of H_2), this translates into an energy requirement of 11322.71 × 0.2211/3600 = 0.6954 W.

A.4. Water vaporization

The specific enthalpy of saturated water (liquid) at 388.70 K is 8727.15 J $\mathrm{mol^{-1}}$, and that of saturated steam (vapor) is 48591.65 J $\mathrm{mol^{-1}}$ [32]. Thus, the energy requirement for vaporization of the feed water at the microreformer inlet pressure of 1.7 atm is

$$(48591.65 - 8727.15)\,\mathrm{J\,mol^{-1}} \times \frac{0.2211}{3600}\,\mathrm{mol\,s^{-1}} = 2.4483\,W. \quad (A.14)$$

A.5. Endothermic heat of reaction

Considering the overall reforming reaction

$$\mathrm{CH_3OH^{(g)} + H_2O^{(g)} \rightleftharpoons CO_2^{(g)} + 3H_2^{(g)}} \quad (A.15)$$

we have:

$$\triangle H_{298.15\,K} = 48.97\,\mathrm{kJ\,mol^{-1}} \quad (A.16)$$

$$\Longrightarrow \triangle H_{245\,^\circ\mathrm{C}} = \triangle H_{518.15\,\mathrm{K}} = \triangle H_{298.15\,K} + \int_{298.15}^{518.15} \triangle C_p(T)\mathrm{d}T = 58.25\,\mathrm{kJ\,mol^{-1}}. \quad (A.17)$$

where

$$\triangle C_p = 3C_{p_{\mathrm{H_2}}}^{(g)} + C_{p_{\mathrm{CO_2}}}^{(g)} - C_{p_{\mathrm{H_2O}}}^{(g)} - C_{p_{\mathrm{CH_3OH}}}^{(g)} \quad (A.18)$$

which is given by [39]:

$$\triangle C_p = 29.655 + 0.149555T - 4.10398 \times 10^{-4}T^2 + 3.34252 \times 10^{-7}T^3 - 9.01766 \times 10^{-11}T^4 \quad (A.19)$$

Thus, the heat requirement for carrying out the endothermic reforming reaction is 58250 × 0.1474/3600 = 2.3850 W.

Appendix B. Supplementary data

Supplementary data associated with this article can be found, in the online version, at 10.1016/j.jpowsour.2005.01.024.

References

[1] P. McFadden, BIOSENSORS: broadband biodetection: holmes on a chip, Science 297 (2002) 2075.
[2] V. Percec, Chemistry: catalyst hunt accelerates, Nature 424 (2003) 135.
[3] T.R. Boussie, G.M. Diamond, C. Goh, K.A. Hall, A.M. LaPointe, M. Leclerc, C. Lund, V. Murphy, J.A.W. Shoemaker, U. Tracht, H. Turner, J. Zhang, T. Uno, R.K. Rosen, J.C. Stevens, A fully integrated high-throughput screening methodology for the discovery of new polyolefin catalysts: discovery of a new class of high temperature single-site group (IV) copolymerization catalysts, J. Am. Chem. Soc. 125 (2003) 4306–4317.
[4] M.A. Burns, B.N. Johnson, S.N. Brahmasandra, K. Handique, J.R. Webster, M. Krishnan, T.S. Sammarco, P.M. Man, D. Jones, D. Heldsinger, C.H. Mastrangelo, D.T. Burke, An integrated nanoliter DNA analysis device, Science 282 (1998) 484–487.
[5] R.F. Service, Shrinking fuel cells promise power in your pocket, Science 296 (2002) 1222.
[6] S. Park, J.M. Vohs, R.J. Gorte, Direct oxidation of hydrocarbons in a solid–oxide fuel cell, Nature 404 (2000) 265–267.
[7] G.A. Deluga, J.R. Salge, L.D. Schmidt, X.E. Verykios, Renewable hydrogen from ethanol by autothermal reforming, Science 303 (2004) 993–997.
[8] L. Schlapbach, A. Zuttel, Hydrogen-storage materials for mobile applications, Nature 414 (2001) 353.
[9] U. Bünger, W. Zittel, Hydrogen storage in carbon nanostructures—still a long road from science to commerce? Appl. Phys. A 72 (2001) 147–151.
[10] P. Pfeifer, M. Fichtner, K. Schubert, M.A. Liauw, G. Emig, Microstructured catalysts for methanol–steam reforming, in: Proceedings of the 3rd International Conference on Microreaction Technology, DECHEMA, Frankfurt, Germany, 1999.
[11] A.Y. Tonkovich, J.L. Zilka, M.J. LaMont, Y. Wang, R.S. Wegeng, Microchannel reactors for fuel processing applications. I. Water gas shift reaction, Chem. Eng. Sci. 54 (1999) 2947–2951.
[12] P.J. de Wild, M.J.F.M. Verhaak, Catalytic production of hydrogen from methanol, Catal. Today 60 1 (2000) 3–10.
[13] S. Fitzgerald, R. Wegeng, A. Tonkovich, Y. Wang, H. Freeman, J. Marco, G. Roberts, D. VanderWeil, A compact steam reforming reactor for use in an automotive fuel processor, in: R.S.W.W. Ehrfeld, I. Rinard (Eds.), Proceedings of the 4th International Conference on Microreaction Technology, Atlanta, GA, 2000, pp. 358–363.
[14] A.V. Pattekar, M.V. Kothare, S.V. Karnik, M.K. Hatalis, A microreactor for in situ hydrogen production by catalytic methanol reforming, in: Proceedings of the 5th International Conference on Microreaction Technology (IMRET 5), Strasbourg, France, 2001.
[15] J.D. Holladay, E.O. Jones, M. Phelps, J. Hu, Microfuel processor for use in a miniature power supply, J. Power Sources 108 (2002) 21.
[16] A.V. Pattekar, M.V. Kothare, Design and fabrication of a microreactor for hydrogen production by catalytic methanol reforming, in: Proceedings of the 2002 AIChE Annual Meeting, Indianapolis, IN, 2002.
[17] M.V. Kothare, A.V. Pattekar, Fuel processing microreactors for hydrogen production by methanol reforming, in: Proceedings of the Knowledge Foundation's 5th International Small Fuel Cells 2003: Small Fuel Cells for Portable Power Applications, New Orleans, LA, 2003.
[18] A.V. Pattekar, M.V. Kothare, Microreactor and method of use to produce hydrogen by methanol reforming, US Patent Pub. App. no. 20040179980. Provisional disclosure filed December, 2002 (in final form: December 2003).
[19] A.V. Pattekar, M.V. Kothare, A microreactor for hydrogen production in micro fuel cell applications, J. Microelectromech. Syst. 13 (2004) 7–18.
[20] M. Richter, A. Drost, J. Kruckow, A high performance silicon micropump for fuel handling in DMFC systems, in: Proceedings of the 2003 Fuel Cell Seminar, Miami beach, FL, 2003.
[21] M.A. Unger, H. Chou, T. Thorsen, A. Scherer, S.R. Quake, Monolithic microfabricated valves and pumps by multilayer soft lithography, Science 288 (2000) 113–116.
[22] W. Qu, I. Mudawar, Measurement and prediction of pressure drop in two-phase micro-channel heat sinks, Int. J. Heat Mass Transfer 46 (2003) 2737–2753.
[23] A.A. Savoretti, D.O. Borio, V. Bucala, J.A. Porras, Non-adiabatic radial-flow reactor for styrene production, Chem. Eng. Sci. 54 (1999) 205–213.
[24] A.V. Pattekar, M.V. Kothare, Novel microfluidic interconnectors for high temperature and pressure applications, J. Micromech. Microeng. 13 (2003) 337–345.
[25] See http://www.lehigh.edu/~asp2/mov/movie-1-uni-flow.wmv for a video of the uniform flow distribution of the fluid exiting the vaporization region (also available as part of supplementary online material at the Journal of Power Sources web-site).
[26] See http://www.lehigh.edu/~asp2/mov/150C-various-flow-rates.wmv for a video of vaporizer operation at 150 °C and various liquid water feed flow rates. (Also available as part of supplementary online material at the Journal of Power Sources web-site).
[27] See http://www.lehigh.edu/~asp2/mov/180C-various-flow-rates.wmv for a video of vaporizer operation at 180 °C and various liquid water feed flow rates. (Also available as part of supplementary online material at the Journal of Power Sources web-site).
[28] See http://www.lehigh.edu/~asp2/mov/200C-various-flow-rates.wmv for a video of vaporizer operation at 200 °C and various liquid water feed flow rates. (Also available as part of supplementary online material at the Journal of Power Sources web-site).
[29] J.C. Amphlett, M.J. Evans, R.A. Jones, R.F. Mann, R.D. Weir, Hydrogen production by the catalytic steam reforming of methanol. Part 1. The thermodynamics, Can. J. Chem. Eng. 59 (1981) 720–727.
[30] W.L. McCabe, J.C. Smith, P. Harriot, Unit Operations of Chemical Engineering, fifth ed., McGraw-Hill, New York, 1993 (Chapter 7).
[31] R.B. Bird, W.E. Stewart, E.N. Lightfoot, Transport Phenomena, Wiley, New York, NY, 1960.
[32] R. Perry, D. Green, Chemical Engineer's Handbook, sixth ed., McGraw-Hill, New York, NY, 1984.
[33] B.A. Peppley, J.C. Amphlett, L.M. Kearns, R.F. Mann, Methanol steam reforming on $Cu/ZnO/Al_2O_3$ catalysts. Part 2. A comprehensive kinetic model, Appl. Catal. A: Gen. 179 (1999) 31–49.
[34] S. Kelley, G. Deluga, W. Smyrl, Miniature fuel cells fabricated on silicon substrates, AIChE J. 48 (2002) 1071–1082.
[35] A.V. Pattekar, M.V. Kothare, Miniature fuel processors and fuel cells for portable power: industry trends and potential applications, in: Proceedings of the 2003 AIChE Annual Meeting, San Francisco, CA, 2003.
[36] See http://www.darpa.mil/dso/thrust/matdev/palmpower/research.html for a summary of the goals of the DARPA palm power project.
[37] Fuel Cell Handbook, sixth ed., EG&G Services Inc., US Department of Energy, Morgantown, WV, November 2002.
[38] A. Schechter, R.F. Savinell, Imidazole and 1-methyl imidazole in phosphoric acid doped polybenzimidazole, electrolyte for fuel cells, Solid State Ionics 147 (2002) 181–187.
[39] C.L. Yaws (Ed.), Chemical Properties Handbook, McGraw-Hill, New York, NY, 1999.